Chinese Journal of Aeronautics 25 (2012) 566-574

Contents lists available at ScienceDirect

Chinese Journal of Aeronautics

journal homepage: www.elsevier.com/locate/cja

A Dual-driven Intelligent Combination Control of Heat Pipe Space Cooling System

LI Yunze[a,*], LI Mingmin[a], LEE Kok Meng[b]

[a] *School of Aeronautic Science and Engineering, Beihang University, Beijing 100191, China*
[b] *George W. Woodruff School of Mechanical Engineering, Georgia Institute of Technology, Atlanta, GA 30332-0405, USA*

Received 30 August 2011; revised 24 October 2011; accepted 4 November 2011

Abstract

Effective thermal control systems are essential for reliable operation of spacecraft. A dual-driven intelligent combination control strategy is proposed to improve the temperate control and heat flux tracking effects. Both temperature regulation and heat flux tracking errors are employed to generate the final control action; their contributions are adaptively adjusted by a fuzzy fusing policy of control actions. To evaluate the control effects, describe a four-nodal mathematical model for analyzing the dynamic characteristics of the controlled heat pipe space cooling system (HP-SCS) consisting of an aluminum-ammonia heat pipe and a variable-emittance micro-electromechanical-system (MEMS) radiator. This dynamical model calculates the mass flow-rate and condensing pressure of the heat pipe working fluid directly from the systemic nodal temperatures, therefore, it is more suitable for control engineering applications. The closed-loop transient performances of four different control schemes have been numerically investigated. The results conclude that the proposed intelligent combination control scheme not only improves the thermal control effects but also benefits the safe operation of HP-SCS.

Keywords: heat pipe; space cooling system; dynamic modeling; intelligent combination control; micro-electromechanical-system

1. Introduction

Heat pipes have been an effective solution for dissipating heat loads of large-package electronic components [1] (such as high quality cache, large HDD, PCMCIA, and new generation mobile PCs [2]), where power density has been rapidly increased to meet stringent requirements of emerging industries. Since the early 2000's, the same trend can be seen in the field of spacecraft thermal control technologies [3-5]. For example, the ALCATEL SPACE in France developed its own axially grooved heat pipes (made of aluminum with ammonia as the working fluid) to meet new thermal-control requirements of future telecommunication and scientific satellites [3]. In Project INTERBALL[4], Kyiv Polytechnic Institute fabricated low-temperature U-shaped heat pipes (with copper shells and capillary structure of metal felt) for the thermal control systems of microsatellites (Magion 4, 5). Heat pipes also play a very important role in the thermal control of large manned spacecraft like international space station (ISS), where ammonia axial-grooved heat pipes (made of aluminum alloy 6063) were designed and tested for the solar battery drives of ISS [5]. Most of these heat pipes were developed as passive thermal control apparatus. To accomplish many tasks that require active thermal control with high precision, future space cooling systems are expected to integrate heat pipes with the newly emerged variable emittance radiators [6-7]. The success of these integrated heat pipe space cooling system (HP-SCS), however, relies on well-designed control policies that requires a good understanding of its open-loop dynamical performances.

More and more investigators have focused on the transient performances and operating characteristics of

*Corresponding author. Tel.: +86-10-82338778.
E-mail address: liyunze@buaa.edu.cn
Foundation item: National Natural Science Foundation of China (50506003)

doi: 10.1016/S1000-9361(11)60420-2

different heat pipe systems since the late 1980's [8-17], which include both experimental approaches [8-9] as well as numerical methods that provide an effective means to simulate the heat pipe dynamics [9-15]. Unsteady distributed models (commonly solved using a finite-deference algorithm) were adopted by early researches [9-11], which are useful bases for analyzing transient performances of micro-grooved heat pipes [12] and flat heat pipes [13] respectively. For control engineering practices, there are needs for simplified mathematical models that can concisely capture the system dynamics for real-time control of heat pipe cooling systems. In Ref. [14], lumped-parameter dynamic models (with experimental validation) were proposed for the entire heat pipe and its nodal sections. Another simplified thermal-network models were proposed in Ref. [15] to describe the transient behavior of the heat pipes using 1st order, linear ordinary differential equations.

The control of a HP-SCS with variable emittance radiators (VER) is an interesting topic that deserves further investigations. Compared to its counterparts, fuzzy logics have several advantages including ease and robustness for characterizing non-linear thermal systems. Fuzzy controllers have been validated for control of nonlinear thermal processes (like hydraulic heating [16] and thermoelectric cooling [17]), and for hybrid fuzzy-PID control of more complex thermal objects (such as boiler plant [18], turbine system [19] and glass melting furnace [20]) by taking advantages of intelligent fuzzy deducing to extend the classical PID technique for improving the system adaptability and robustness, and ease practical implementation. Since heat transfer mechanics within a heat pipe and at the surface of variable emittance micro-electromechanical-system (MEMS) radiator are typically nonlinear, controllers employing fuzzy logic become promising candidates for effective control of HP-SCS.

This paper presents an intelligent combination control strategy where the control decision is driven simultaneously by a pair of err signals (the temperature control err of the object being cooled and the heat flux tracking err of the radiator) to provide a direct yet smoother control effect than the control scheme driven by a single err signal (either temperature or by heat flux). Finally, the closed-loop control performances are numerically analysed and discussed.

2. Mathematical Model of Controlled HP-SCS

2.1. Descriptions of controlled system

Figure 1(a) shows the HP-SCS that consists of an aluminum-ammonia heat pipe and a VER with a MEMS louver array. The exhaust heat from the electronic components inside the spacecraft is collected by the evaporator section of the heat pipe, which is then transferred to the VER commonly placed outside of the spacecraft. The exhaust heat is finally dissipated into the space environment by heat radiation; the MEMS louver on the radiator provides a means to adjust its cooling ability.

1) Heat pipe mechanism (see Fig. 1(b))

The aluminum-ammonia heat pipe considered here comprises an evaporator section (ES), an adiabatic section (AS) and a condenser section (CS). A tubular wick (a capillary structure) is filled with liquid ammonia as a working fluid inside the aluminum container. When the ES is heated by the external heat, the liquid ammonia inside it changes from liquid to vapor, and then rushes to the CS through the vapor cavum of heat pipe. Heat leaves the heat pipe and the working fluid is chilled into liquid at the CS. This chilled liquid working fluid is pumped back to the ES by the capillary structure.

2) Variable emittance MEMS radiator (see Fig. 1(c))

The cooling behavior of the VER is dominated by heat radiation since there is no air outside the in-orbit spacecraft. An MEMS louver array is mounted on the radiator surface with high-emittance (HE-RS) to control the leaving heat flux. When a louver cell in the MEMS array is opened, the HE-RS under it is exposed to the space environment; otherwise, the low-emittance surface (LES) of the cover faces the space. Therefore, the cooling ability of heat pipe cooling system can be controlled by simply adjusting the number of opening louver cells. We define the exposing degree μ_r as the ratio between the exposed area and the total area of radiator surface.

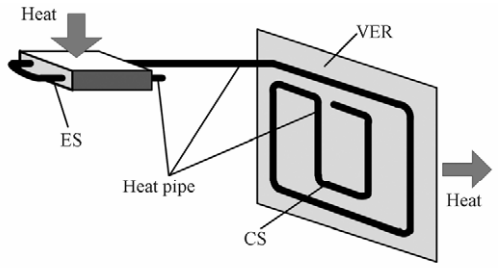

(a) Scheme of the HP-SCS

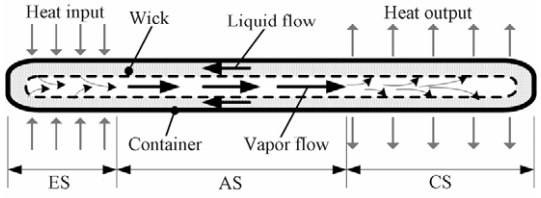

(b) Heat pipe machnism

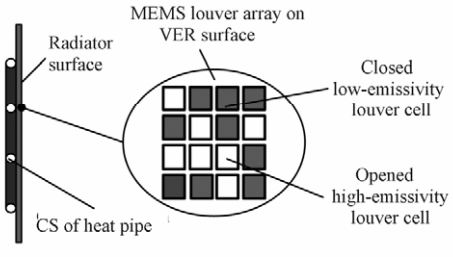

(c) Radiator with MEMS louver array

Fig. 1 HP-SCS and its components.

The heat flux leaving the radiator can be approximated by

$$Q_r = \varepsilon_e \sigma A_r T_r^4 = \left[(\varepsilon_h - \varepsilon_l)\mu_r + \varepsilon_l\right]\sigma A_r T_r^4 \quad (1)$$

where σ is the Stefan-Boltzmann constant, and ε_e the equivalent emittance of the radiator, ε_h and ε_l are the emittance of the HE-RS and the MEMS louver cell covering it, and A_r and T_r the total area and average temperature of radiator surface.

2.2. Mathematical model

HP-SCS typically operate in a vacuum in-orbit environment with cold background temperature (of lower than 4 K in space) [21], a condition very different from that at the earth surface. Complex thermal vacuum facilities [22] or other equivalent physical simulators [17] are often required for any ground-based experiments for simulating the space cooling behavior characterized by Eq. (1). For a transient performance test, the dynamic characteristics of the employed space simulators must be specially considered and strictly controlled [17], usually more complex and difficult to be achieved than that of the HP-SCS itself. Therefore, mathematical modeling and numerical investigation are very important for understanding the close-loop transient performances of the HP-SCS before a ground-based or real in-orbit-flying test is available.

Insightful assumptions are necessary in order to develop a relatively simple model without compromising essential dynamical information [23]. Two assumptions are made in modeling the HP-SCS.

1) Modeling assumptions

At present, the power densities of the objects inside modern spacecraft to be cooled reach the level of 20 W/cm^2 [4] while the maximum blackbody heat dissipating abilities at the radiator surface are only about 0.05 W/cm^2 at normal temperature of 300 K according to Eq. (1). Large radiator areas and long CS in the heat pipe are required to meet the requirements of the in-orbit heat dissipating task. As a result, the thermal inertia with the CS is much larger than that impacted on the ES. Thus, according to the investigations in Ref. [23], the relationship between the transient temperature changes of the CS and those of the whole heat pipe can be approximated by:

$$\mathrm{d}T_c/\mathrm{d}\tau \approx \mathrm{d}T_{hp}/\mathrm{d}\tau \quad (2)$$

where T_c is the condenser temperature, and T_{hp} the average temperature of the CS and those of the entire heat pipe respectively.

Moreover, the vapor density is much smaller than that of the liquid inside the small working fluid volume V_{wl} of the wick. The density variation of the saturated liquid with temperature changes is also very small [24]. Additionally, the temperature changes with the entire heat pipe and its ES and CS are slow (with settling times usually much longer than several minutes based on published results in Refs. [9]-[11] and Ref. [15]). Therefore, the mass flow-rate imbalance caused by the heat pipe temperature changes can be neglected as compared to the cycling mass flow rate determined by the cooling ability [23]:

$$\frac{|G_l - G_v|}{Q_i/(h_v - h_l)} = \frac{(h_v - h_l)V_{wl}}{Q_i}\cdot\left|\left(\frac{\mathrm{d}\rho_l}{\mathrm{d}T_{hp}}\right)\left(\frac{\mathrm{d}T_{hp}}{\mathrm{d}\tau}\right)\right| \quad (3)$$

where ρ_l, h_v and h_l are the liquid density, vapor enthalpy and liquid enthalpy of the working fluid at the saturated state, G_l and G_v the liquid and vapor mass flow-rates, Q_i is the input heat load. Thus, G_l and G_v inside the heat pipe approximately satisfy

$$G_l = G_v = G_{hp} \quad (4)$$

where G_{hp} is the cycling mass flow-rate of the working fluid in the heat pipe.

2) Dynamical temperature equations

Since the temperature dynamics of the heat pipe can be modeled by either one or several lumped-parameter nodes [14-15,23-24], the heat pipe is divided here into two lumped-parameter nodes and the whole HP-SCS is modeled as a four-nodal thermal network illustrated in Fig. 2(a). The nodal temperatures of the object, the CS and ES of the heat pipe and the radiator are governed by their respective energy conservation equations given in Eqs. (5)-(8):

A) For the absolute temperature of the cooled object (with thermal capacity C_{ob}), T_{ob}:

$$C_{ob}\dot{T}_{ob} = Q_i - (T_{ob} - T_e)/R_{oe} \quad (5)$$

where T_e is the absolute temperature of ES, and R_{oe} the thermal resistance between the object and ES.

B) For the ES (with thermal capacity C_e):

$$C_e\dot{T}_e = (T_{ob} - T_e)/R_{oe} - G_{hp}(h_v - h_l) \quad (6)$$

C) Similarly, for the condenser temperature T_c of the CS (with thermal capacity C_c):

$$C_c\dot{T}_c = G_{hp}(h_v - h_l) - (T_c - T_r)/R_{cr} \quad (7)$$

where R_{cr} is the thermal resistance between the condenser and radiator, the determination of C_c and C_e can be referred to Ref. [14].

D) The temperature of the radiator (with thermal capacity C_r) can be solved from

$$C_r\dot{T}_r = (T_c - T_r)/R_{cr} + Q_{ex} - Q_r \quad (8)$$

where Q_{ex} is the part of external radiation heat load from the sun and earth received by the radiator [21], the dissipative heat Q_r from the radiator to space has been given in Eq. (1).

3) Mass flow rate and condensing pressure algorithm

However, the calculation of the temperature transient from Eqs. (5)-(8) requires the determination of G_{hp}. For this, we deduce the CS temperature by treating the entire heat pipe as one node [14] so that the HP-SCS dynamic model can be reduced to a three-node thermal network (see Fig. 2(b)). With the Eq. (2), the CS

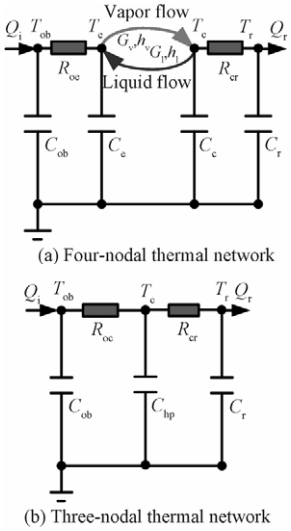

Fig. 2 Thermal network models of HP-SCS.

temperature can be determined from the energy conservation equation at the T_c node in the three-node thermal network [23]:

$$\dot{T}_c \approx \dot{T}_{hp} = \frac{1}{C_{hp}}\left[(T_{ob}-T_c)/R_{oc}-(T_c-T_r)/R_{cr}\right] \quad (9)$$

where C_{hp} is the thermal capacity of the entire heat pipe, and R_{oc} (R_{oc}=R_{hp}+R_{oe}) the thermal resistance between the cooled object and CS. The substitution of Eq. (9) into Eq. (7) yields a closed-form equation for computing G_{hp} in terms of the transient nodal temperatures:

$$G_{hp} = \frac{1}{h_v-h_l}\cdot\left[\frac{C_c}{C_{hp}}\cdot\frac{(T_{ob}-T_c)}{R_{oc}}+\left(1-\frac{C_c}{C_{hp}}\right)\cdot\frac{(T_c-T_r)}{R_{cr}}\right] \quad (10)$$

Using T_c as the representative temperature of the working fluid since the CS may contain more fluid than the ES, the saturated pressure p_c of the working fluid inside the heat pipe is given by Eq. (11), a curve-fit polynomial using data published in Ref. [23] and Ref. [25]:

$$p_c = \sum_{i=1}^{6} A_i (T_c - 273.15)^{i-1} \quad (11)$$

where the coefficients A_i (i=1, 2, …, 6) for ammonia as working fluid are listed in Table A1 in the Appendix.

3. Intelligent Combination Control Strategies

3.1. Block diagrams and control algorithms

The primary purpose of the spacecraft thermal control is to keep the thermal balance between the heat emission with cooled objects and the heat dissipation at radiator surfaces, while maintaining the working temperature of the cooled object for a safe operation [21]. The temperature of the cooled object is the most widely adopted controlled variable as it is easily measurable and perfect set-point control effects. However, the temperature-driven controllers are not as sensitive as the controllers directly driven by the heat flux tracking err between the radiator and cooled object. Unfortunately, the latter cannot realize the set-point control of the cooled object temperature.

To ensure the HP-SCS to have a good set-point temperature control with a fast and stable heat flux tracking ability, we develop a temperature-heat intelligent combination-control (TQ-ICC) scheme driven simultaneously by the temperature controlling err and the heat-flux tracking err to generate an optimized control action as shown in Fig. 3(a).

As shown in Fig. 3(b), the proposed TQ-ICC consists of a dual-driven control unit and a fuzzy fusing unit (FFU). The temperature control err e_t and the heat flux tracking err e_q are fed to the dual-driven control unit. The two virtual controlling variable increments ($\Delta\mu_{rt}$ and $\Delta\mu_{rq}$) are produced by the temperature- driven PID (T-PID) controllers and heat-flux-driven PID (Q-PID) controllers, respectively.

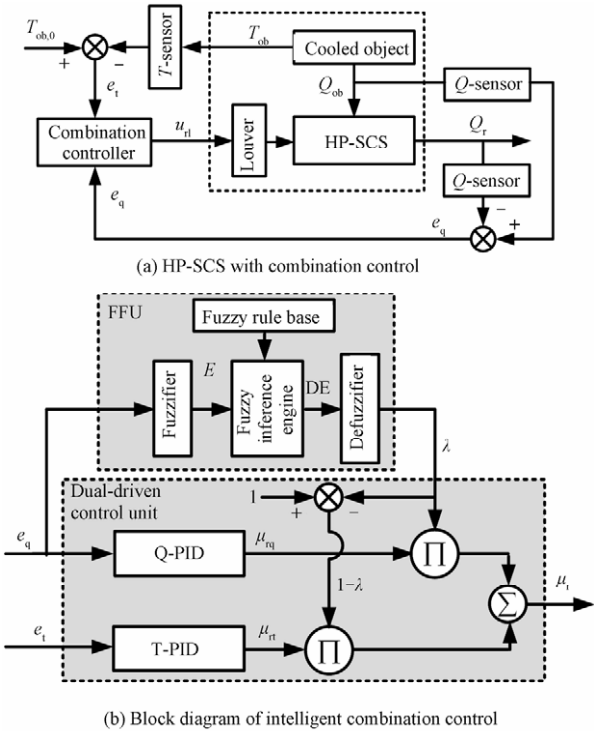

Fig. 3 Intelligent combination control.

The T-PID is a temperature set-point controller where its virtual increment $\Delta\mu_{rt}$ is calculated from the e_t between referenced and measured temperatures of the cooled object:

$$\Delta\mu_{rt,k} = K_{p,t}\begin{bmatrix}1 & \frac{T_s}{T_{i,t}} & \frac{T_{d,t}}{T_s}\end{bmatrix}\begin{bmatrix}e_{t,k}-e_{t,k-1}\\ e_{t,k}\\ e_{t,k}-2e_{t,k-1}+e_{t,k-2}\end{bmatrix} \quad (12)$$

Similarly, the virtual increment $\Delta\mu_{rq}$ of the Q-PID controller is calculated from the e_q between the exhaust heat of the cooled object and the cooling heat flux of

the radiator:

$$\Delta\mu_{\mathrm{rq},k} = K_{\mathrm{p,q}}\left[1 \quad \frac{T_\mathrm{s}}{T_{\mathrm{i,q}}} \quad \frac{T_{\mathrm{d,q}}}{T_\mathrm{s}}\right]\begin{bmatrix} e_{\mathrm{q},k} - e_{\mathrm{q},k-1} \\ e_{\mathrm{q},k} \\ e_{\mathrm{q},k} - 2e_{\mathrm{q},k-1} + e_{\mathrm{q},k-2} \end{bmatrix} \tag{13}$$

In Eqs. (12)-(13), the subscripts, k, k–1 and k–2, represent the values at kth, (k–1)th and (k–2)th instants, and the subscripts t and q indicate that the proportional gain K_p, integral time T_i and derivative time T_d refer to the T-PID and Q-PID respectively, T_s is the sampling period.

Finally, the actual controlling variable $\Delta\mu_\mathrm{r}$ (at the current sampling time k) is determined by the following fusing law:

$$\mu_{\mathrm{r},k} = \mu_{\mathrm{r},k-1} + \lambda_k\Delta\mu_{\mathrm{rq},k} + (1-\lambda_k)\Delta\mu_{\mathrm{rt},k} \tag{14}$$

where λ_k is the fusing factor and $0 \le \lambda_k \le 1$.

The fusing factor λ_k provides a means to adjust the relative contributions of $\Delta\mu_\mathrm{rt}$ and $\Delta\mu_\mathrm{rq}$ according to the instantaneous control situation. Since the heat balance is the major thermal control task, Q-PID is more effective when e_q is large. On the other hand, the set-point temperature control becomes more important when e_q is small (note that small e_q does not mean a small e_t). The fundamental policy for determining λ_k is that large λ_k is assigned for large heat flux tracking err. A graphic for a better understanding of the preliminary fusing factor generating policy is given in Fig. 4.

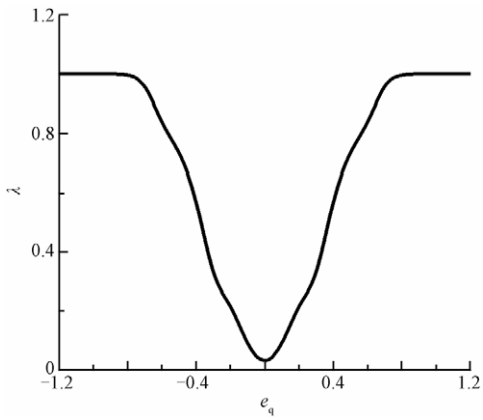

Fig. 4 Control action fusing factor.

The parameter settings of the T-PID and Q-PID in Eq. (12) and Eq. (13) can be respectively designed using traditional tuning methods [26] by treating them as independent PID controllers, since better independent temperature control or heat flux tracking effects lead to better combination control effect once the fusing factor generating policy is given.

3.2. Fuzzy fusing unit (FFU)

The FFU shown in Fig. 3(b) consists of a fuzzifier, a defuzzifier, a fuzzy inference engine and a fuzzy rule-base for generating the linguistic fusing factors. The fuzzy sets and linguistic values are summarized in Table 1; to simplify analyses and programming, each fuzzy set is given an analytical rank and a Gaussian membership function (see Fig. 5).

Table 1 Fuzzy sets and their linguistic values

Fuzzy set	Rank	Linguistic value
NG	–4	Negative great
NL	–3	Negative large
NM	–2	Negative medium
NS	–1	Negative small
PG	4	Positive great
PL	3	Positive large
PM	2	Positive medium
PS	1	Positive small

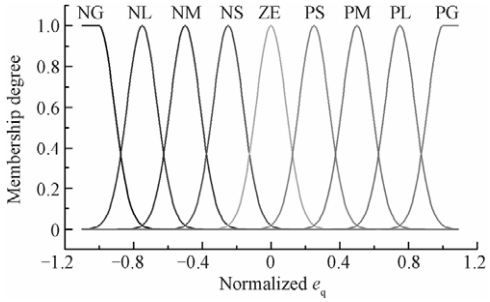

Fig. 5 Membership functions for fuzzy sets.

Each fusing rule in the rule-base takes a general form: if $e_{\mathrm{q},k}$ is E_i, then λ_k is $\mathrm{DE}_{j(i)}$. E_i and $\mathrm{DE}_{j(i)}$ are the fuzzy sets which represent linguistic values of $e_{\mathrm{q},k}$ and λ_k respectively; the subscript variables i, $j(i)$ denote the analytical ranks associated with these linguistic values in Table 1.

Since a large fusing factor is required for large heat flux tracking err while a small fusing factor is expected in the situations of small tracking err, we construct the fuzzy rules for the fusing of virtual control actions using a rank-based rule-generating policy derived in:

$$j(i) = \mathrm{nInt}(\alpha[1-\exp(-i^2/\beta^2)]) \tag{15}$$

where the output of the function nInt (x) is the nearest integer number of the input x. In Eq. (15), the values of α and β are set to 4.0 and 1.5 which are chosen after a series of numerical simulations. For this one-input system ($e_{\mathrm{q},k}$ with nine fuzzy values), the fully populated rule base has nine fusing rule combinations (see Table 2).

Table 2 Fuzzy fusing rules

E_i	NG	NL	NM	NS	ZE	PS	PM	PL	PG
$\mathrm{DE}_{j(i)}$	PG	PG	PL	PS	ZE	PS	PL	PG	PG

The fusing factor from the fuzzy fusing rules is then

given by the following defuzzification algorithm in the form of

$$\lambda_k = \sum_{i=1}^{9} \lambda_{\mathrm{r},j(i)} \omega_{j(i)} \Big/ \sum_{j=1}^{9} \omega_{j(i)} \tag{16}$$

where $\lambda_{\mathrm{r},j(i)}$ and $\omega_{j(i)}$ are the representative discrete element and membership degree of the output fuzzy set $\mathrm{DE}_{j(i)}$.

In fact, before using the fuzzy rules mentioned above, the fuzzy fusing process on error and error increment should be conducted, in another word, the membership degree of the output fuzzy set (E_i, $\mathrm{DE}_{j(i)}$) on given double input (error, error increment) is calculated based on the function as is shown in Fig. 2. The equation of the $\omega_{j(i)}$ is given by :

$$\mu(x,k) = \exp\left(\frac{x-(k\times a)}{b} \right)^2 \tag{17}$$

where $k\in\{i, j\}$; $x\in\{e, e_c\}$, a is set to 0.25, and the value of b could be regulated and is set to 0.125 here. When x exceed the range (−1, 1), $\omega_{j(i)}$ is given by

$$\begin{cases} \mu(x,-4)=1, & x<-1 \\ \mu(x,\ 4)=1, & x>1 \end{cases} \tag{18}$$

The fuzzy generated fusing factor value for the different heat flux tracking err is plotted in Fig. 4. Using this intelligent fusing policy for the control action, the Q-PID dominates the response of MEMS radiator when e_q is large and the temperature-driven T-PID governs the control action when e_q becomes small; thus, the proposed TQ-ICC combines the advantages of both the Q-PID and T-PID. Moreover, unlike traditional split-range controllers, the TQ-ICC in any operating situation whether the value of e_q is large or small, and their contributions in Eq. (14) can be adaptively, stably and continuously adjusted.

When designing an actual control system for the HP-SCS focused in this paper, major tasks are to determine the parameters in Eqs. (13)-(15) and Eq. (17). As what already stated in the descriptions of these equations, the values of the patameters above are reached through mumercial simulaton trials which are recommended by Refs. [26]-[27].

4. Simulation Results and Discussions

4.1. System parameters and simulated cases

To evaluate the intelligent combination control action, four different control schemes are numerically compared:

Scheme I Single temperature-driven T-PID controller without the contributions of Q-PID and FFU.

Scheme II Pure heat flux driven Q-PID controller with no intervention from T-PID or FFU.

Scheme III Combination control with the preliminary fusing law in Eq. (15), here denotes as TQ-PCC.

Scheme IV TQ-ICC with the fuzzy fusing law in Eq. (16) and Table 2.

The parameters for the single input T-PID and Q-PID in Schemes I and II are set at their best-performance values founded by close-loop numerical simulation trials. For faith and reasonable comparisons, the same groups of parameters are applied to the corresponding T-PIDs and Q-PIDs inside dual-driven TQ-PCC and TQ-ICC as shown in Table 3. The values used in the simulated system and its working fluid parameters are summarized in Table A2 and Table A2 in the Appendix. A +10% step change with the input heat load Q_i is fed to the above active controllers during numerical investigations.

Table 3 Parameters of simulated controllers

Parameter	Value (for Schemes I, III and IV)	Parameter	Value (for Schemes II, III and IV)
$K_{p,t}$	1.5	$K_{p,q}$	−2.0
$T_{i,t}$	15.0	$T_{i,q}$	160.0
$T_{d,t}$	0	$T_{d,q}$	0.001

Note: sampling period, T_S = 1.0 s, these values are for normalized input/output signals.

4.2. Intelligent combination control effects

Numerical results are graphed in Figs. 6-9, and the quality indexes including settling time and overshoot (denote as τ and σ respectively) for different responses have been calculated from the numerical results and compared in Table 4. The widely adopted single temperature-driven T-PID (in Scheme I) serves as a basis for comparisons.

Table 4 Settling times and overshoots of closed-loop responses

Parameter	Scheme Ⅰ		Scheme Ⅱ	Scheme Ⅲ		Scheme Ⅳ	
	τ^*/s	σ^*	τ/τ_I	τ/τ_I	σ/σ_I	τ/τ_I	σ/σ_I
T_{ob}	1 071	4.5	0.141	0.865	0.934	0.757	0.891
T_r	947	−1.2	0.034	0.786	0.471	0.627	0.245
T_e	1 105	4.6	0.137	0.604	0.881	0.726	0.859
T_c	886	−0.8	0.036	0.821	0.472	0.708	0.226
Q_r	837	9.5	0.149	0.817	0.499	0.878	0.397
μ_r	888	6.2	0.141	0.827	0.534	0.594	0.301
P_c	893	2.7	0.035	0.833	0.757	0.646	0.242
G_{hp}	427	3.8	0.332	0.902	0.600	0.623	0.533

Note: 1) error band of τ are 0.5 K for temperatures and 2% final value for others;

2) units for σ are 'K' for temperatures and '%' for others.

Observations are summarized as follows:

1) Temperature and heat flux control effects

The added heat flux signal into the temperature control system improves the control effects of TQ-ICC by shortening settling times and reducing overshoots.

A) Although the Q-PID in Scheme II responds most

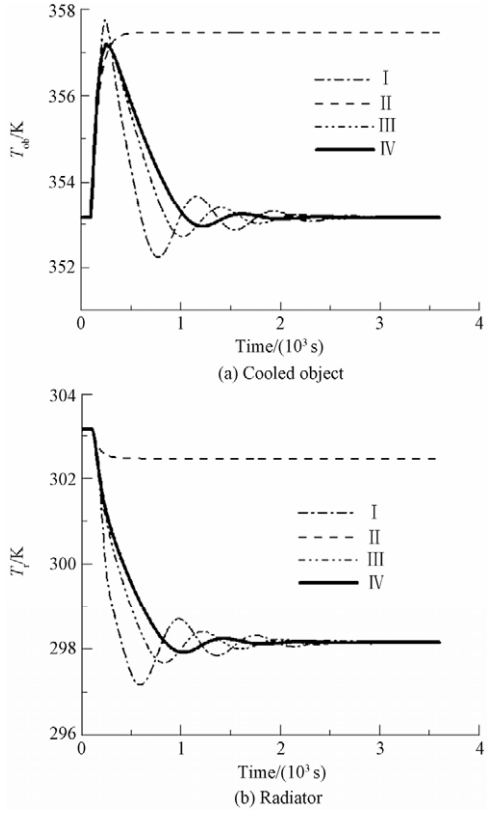

Fig. 6 Control effects on the temperatures of cooled object and radiator.

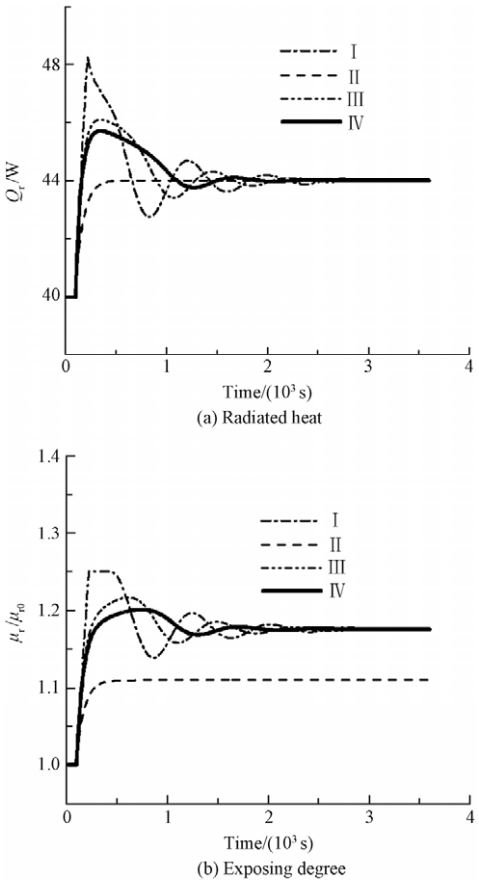

Fig. 7 Heat flux tracking effects and exposing degree responses.

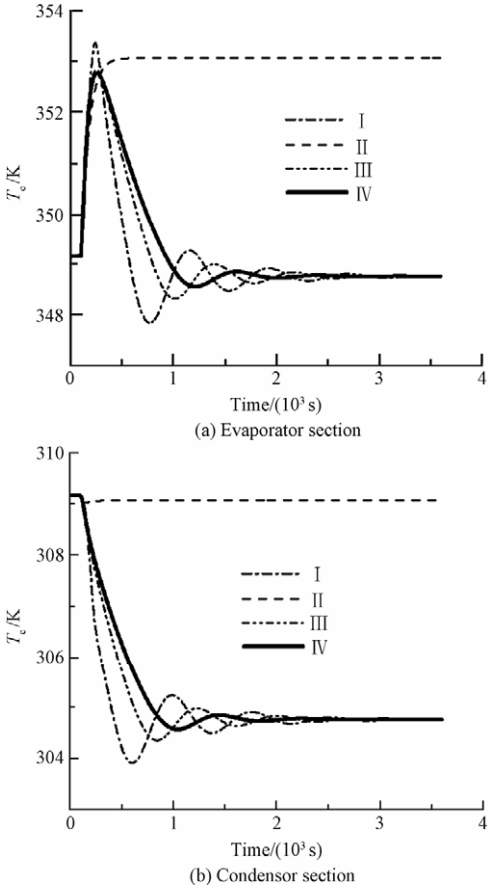

Fig. 8 Reponses of heat pipe temperatures.

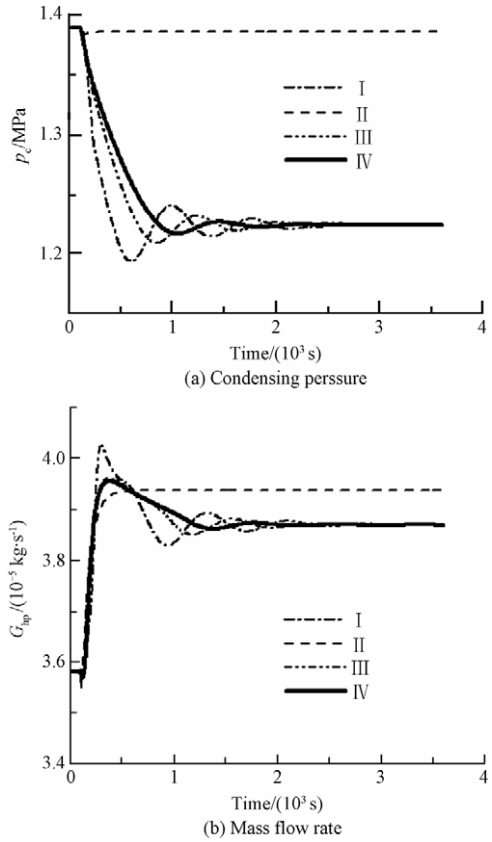

Fig. 9 Controlled hydraulic transient inside heat pipe.

quickly (Q_r in Fig. 7(a)) with a settling time of only 14.1 % of the base-case T-PID, it cannot control T_{ob} (in Fig. 6(a)) at its reference value but with a final offset of 4.29 K.

B) Both dual-driven combination controls in Schemes III and IV achieve the objectives of temperature control and heat flux tracking successfully. Compared with the T-PID in Scheme I, the corresponding settling times of T_{ob} are shortened to 86.5% and 75.7% by TQ-PCC and TQ-ICC, while reducing the overshoots of Q_r to 49.9% and 39.7% respectively.

C) The radiator temperatures (T_r in Fig. 6(b)) in all Schemes (I to IV) drop to their new stable values, yet the smallest temperature decrease is with Q-PID in Scheme II (only about 0.7 K). The final decreases for the other three schemes are the same (of about 5 K). The overshoot of T_r under TQ-ICC is only 24.5% of that with T-PID in Scheme I.

D) The smallest μ_r change (in Fig. 7(b)) is only 11% with the Q-PID in Scheme II while the final changes for Schemes I, III and IV all are 17.6%. The smallest overshoot among the last three schemes is with the proposed TQ-ICC, and the corresponding value is only 30.1% of the most widely adopted T-PID in Scheme I.

2) Heat pipe responses

The heat flux signals also reduce the temperature and pressure oscillation in the heat pipe.

A) Although the ES temperatures (T_e in Fig. 8(a)) drop to the same final value (of 0.4 K lower than the initial state) under Schemes I, III and IV, the overshoot and settling time of proposed TQ-ICC are only 85.9% and 72.6% of the corresponding values of the T-PID in Scheme I. Similar improvements are found with the changes of T_c in Fig. 8(b), and the overshoot of TQ-ICC is only 22.6 % of the base-case single T-PID.

B) For the condensing pressure (p_c, in Fig. 9(a)), the proposed TQ-ICC shortens pressure oscillation process to 64.6% and reduces the overshoot to 24.2% of the respective values of single T-PID. This is essential for the safe operation of heat pipe in the vacuum space environment.

C) The overshot and settling time of G_{hp} with proposed TQ-ICC are only 53.3% and 62.3% of the corresponding values of the T-PID in Scheme I, while the final increases of G_{hp} all are 7.6 % (in Fig. 9(b)) under Schemes I, III and IV. Therefore the change of G_{hp} under TQ-ICC is more stable.

Since the pure Q-PID in Scheme II results in an unexpected temperature rise with T_{ob} and T_e in Fig. 6(a) and Fig. 8(a) respectively, it is not suitable for the applications where high-precision temperature control is required.

5. Conclusions

This paper offers a detailed analysis and a method to control a HP-SCS comprising of an aluminum-ammonia heat pipe and a variable-emittance MEMS radiator.

1) A four-node dynamical model has been presented. The model calculates the mass flow rate of the heat pipe working fluid immediately from the systemic nodal temperatures. This simplifies the transient analysis of the whole HP-SCS for control engineering applications.

2) The intelligent combination control strategy TQ-ICC improves the thermal control effects by adding a heat flux tracking err to the proposed dual driven system and adaptive adjustment of the contributions from the temperature controlling and heat flux tracking errs.

3) Comparisons between the four simulated control schemes support the fact that the proposed TQ-ICC takes advantages of short settling time with small overshoot as compared to traditional T-PID based control (only 75.7% and 89.1% of the base-case T-PID for T_{ob}).

Numerical results presented here are expected to be valuable for control system design of a HP-SCS especially when the over-expensive ground-based or real in-orbit flying experiments are not available.

References

[1] Zuo Z J, North M T, Wert K L. High heat flux heat pipe mechanism for cooling of electronics. IEEE Transactions on Components and Packaging Technologies 2001; 24(2): 220-225.

[2] Nguyen T, Mochizuki M, Mashiko K, et al. Advanced cooling system using miniature heat pipes in mobile PC. IEEE Transactions on Components and Packaging Technologies 2000; 23(1): 86-90 .

[3] Hoa C, Demolder B, Alexandre A. Roadmap for developing heat pipes for ALCATEL SPACE's satellites. Applied Thermal Engineering 2003; 23(9): 1099-1108.

[4] Baturkin V, Zhuk S, Vojta J, et al. Elaboration of thermal control systems on heat pipes for microsatellites Magion 4, 5 and BIRD. Applied Thermal Engineering 2003; 23(9): 1109-1117.

[5] Barantsevich V, Shabalkin V. Heat pipes for thermal control of ISS solar battery drive. Applied Thermal Engineering 2003; 23(9): 1119-1123.

[6] Osiander R, Firebaugh S L, Champion J L, et al. Microelectromechanical devices for satellite thermal control. IEEE Sensors Journal 2004; 4(4): 525-531.

[7] Farrar D, Schneider W, Osiander R, et al. Controlling variable emittance (MEMS) coatings for space applications. The Eighth Intersociety Conference on Thermal and Thermomechanical Phenomena in Electronic Systems, 2002; 1020-1024.

[8] El-Genk M S, Huang L, Tourniert J M. Transient experiments of an inclined copper-water heat pipe. Journal of Thermophys and Heat Transfer 1995; 9(1): 109-116.

[9] Bowman J, Sweeten R. Numerical heat-pipe modeling. 24th AIAA Thermophysics Conference, 1989; 12-14.

[10] Bowman W J. Numerical modeling of heat-pipe transients. Journal of Thermophys and Heat Transfer 1991; 5(3): 374-379.

[11] Chang W S, Leland J E. Finite difference simulation of transient heat pipe operation. 27th Aerospace Sciences Meeting, 1989.

[12] Suman B, De S, Gupta S D. Transient modeling of

micro-grooved heat pipe. International Journal of Heat and Mass Transfer 2005; 48(8): 1633-1646.
[13] Sonan R, Harmand S, PelléJ, et al. Transient thermal and hydrodynamic model of flat heat pipe for the cooling of electronics components. International Journal of Heat and Mass Transfer 2008; 51(25-26): 6006-6017.
[14] Tilton D E, Chow L C, Mahefkey E T. Transient response of a liquid metal heat pipe subjected to external thermal loading at the condenser. 4th AIAA and ASME, Joint Thermophysics and Heat Transfer Conference, 1986.
[15] Zuo J, Faghri A. A network thermodynamic analysis of the heat pipe. International Journal of Heat and Mass Transfer 1998; 41(11): 1473-1484.
[16] Haissig C. Adaptive fuzzy temperature control for hydronic heating systems. IEEE Control Systems 2000; 20(2): 39-48.
[17] Li Y Z, Lee K M, Wang J. Analysis and Control of Equivalent Physical Simulator for Nanosatellite Space Radiator. IEEE/ASME Transactions on Mechatronics 2010; 15(1): 79-87.
[18] Wang W, Li H X, Zhang J. Intelligence-based hybrid control for power plant boiler. IEEE Transactions on Control Systems Technology 2002; 10(2): 280-287.
[19] Li H, Liu H, Cai W J, et al. A new coordinated control strategy for boiler-turbine system of coal-fired power plant. IEEE Transactions on Control Systems Technology 2005; 13(6): 943-954.
[20] Moon U C, Lee K Y. Hybrid algorithm with fuzzy system and conventional PI control for the temperature control of TV glass furnace. IEEE Transactions on Control Systems Technology 2003; 11(4): 548-554.
[21] Gilmore D G. Spacecraft thermal control handbook. 2nd ed. California: The Aerospace Press, 2002.
[22] Rouse J A, Corinth R L. Meeting today's requirements for large thermal vacuum test facilities. 4th Space Simulation Conference, 1986, 112-130.
[23] Li Y Z, Wang Y Y, Lee K M. Dynamic modeling and transient performance analysis of a LHP-MEMS thermal management system for spacecraft electronics. IEEE Transactions on Components and Packaging Technologies 2010; 33(3): 597-606.
[24] Faghri A, Harley C. Transient lumped heat pipe analysis. Heat Recovery Systems & CHP 1994; 14(4): 351-363.
[25] Wei C B, Lu S X, Zhou Z Y. Practical handbook of refrigeration and air-conditioning engineering. Beijing: China Machine Press, 2006; 1-32. [in Chinese]
[26] Luyben W L. Process modeling, simulation and control for chemical engineers. New York : McGraw-Hill Publisbing Company, 1990; 231-238.
[27] Kovacic Z, Bogdan S. Fuzzy controller design theory and applications. Boca Raton: Taylor & Francis Group, 2006; 75-110.

Appendix

Table A1 Parameters of pressure equation of working fluid

Parameter	Value	Parameter	Value
A_1	$4.293\ 025\times10^{-1}$	A_4	$1.558\ 870\times10^{-6}$
A_2	$1.605\ 853\times10^{-2}$	A_5	$2.940\ 981\times10^{-9}$
A_3	$2.351\ 689\times10^{-4}$	A_6	$1.322\ 185\times10^{-12}$

Table A2 Simulated HP-SCS

Design working parameter	Symbol	Value
Cooling ability/W	Q_i	40
Cooled object temperature/K	T_{ob}	353.15
Radiator temperature/K	T_r	303.15
Heat pipe condensing temperature/K	T_c	309.15
System characteristic parameter	**Symbol**	**Value**
Thermal capacity of cooled object/($J\cdot K^{-1}$)	C_{ob}	45.2
Thermal capacity of radiator/($J\cdot K^{-1}$)	C_r	135.6
Thermal resistance of heat pipe/($K\cdot W^{-1}$)	R_{hp}	1.0
Thermal resistance between cooled object and heat pipe/($K\cdot W^{-1}$)	R_{oe}	0.1
Thermal resistance between heat pipe and radiator/($K\cdot W^{-1}$)	R_{cr}	0.15

Biographies:

LI Yunze received the Ph.D. degree in engineering thermal physics from Tsinghua University in 2002. Currently, he is a professor with the School of Aeronautic Science and Engineering, Beihang University, Beijing. His current major research interests include thermal control and energy management of aerospace systems.
E-mail: liyunze@buaa.edu.cn

LI Mingmin received the Master degree from the School of Aeronautic Science and Engineering, Beihang University, Beijing. Her major research interest is the heat control of the onboard systems of advanced spacecraft.
E-mail: limingmin@buaa.edu.cn

LEE Kok Meng received the M.S. and Ph.D. degrees from the Massachusetts Institute of Technology, Cambridge, in 1982 and 1985, respectively. Currently, he is a professor with the Woodruff School of Mechanical Engineering, Georgia Institute of Technology, Atlanta. His current research interests include system dynamics control, robotics, automation, and mechatronics.
E-mail: kokmeng.lee@me.gatech.edu